MATERIAL NORMAL ENERGY DISTRIBUTION FOR FIELD EMISSION ANALYSES FROM MONOCRYSTALLINE SURFACES*

J. I. Mann[†], Y. Li, J. B. Rosenzweig, UCLA, Los Angeles, CA 90024, USA

J. K. Nangoi, T. Arias, Cornell University, Ithaca, NY 14850, USA

Abstract

Electron field emission is a complicated phenomenon which is sensitive not only to the particular material under illumination but also to the specific crystalline orientation of the surface. Summarizing the ability for a crystal to emit in a particular direction would be of great use when searching for good field emitters. In this paper we propose a material normal energy distribution which describes the ability of the bound electrons to tunnel under an intense electric field. This framework breaks a computationally expensive 3-D system down to a source distribution representation applicable for more efficient 1-D models. We use the Fowler-Nordheim framework to study the yield and MTE (mean transverse energy) from sources including gold, copper, and tungsten in both monocrystalline and polycrystalline forms. We find an increase in effective work function for field emission in the (111) direction for gold and copper associated with the Bragg plane intersections of the Fermi surface.

INTRODUCTION

Electrons are commonly sourced through field emission. Nanotips, for instance, are used in a static field emission setup for electron microscopy [1]. Field emission is also the culprit of dark current [2] and may lead to breakdown [3] in RF cavities. Strong laser field emission is a growing topic of interest where a nanostructured cathode is used to enhance laser fields to field-emitting regimes [4].

Field emission is typically analyzed in 1-D using the Fowler-Nordheim (FN) framework [5] where each electron impinging on the surface has a probability of tunneling and emitting. This probability, for a transversely isotropic surface potential, is invariable on the transverse momentum and is therefore only dependent on the normal energy, summarized by the vacuum motive energy $M(x) = U(x) - E_n$ with U the vacuum potential and E_n the energy directed normal to the surface. The motive energy is integrated within the classically forbidden region to determine the tunneling probability. It is thusly important to understand the distribution of source current within the material with respect to the normal energy when finding the field emission current.

The FN model for field emission is typically considered using an isotropic free electron gas (FEG) scheme. In this case, there is a constant current density in energy space, permitting simple analytical results in the limits of low or high field strength [5]. However, we do not expect all crystalline surfaces to behave like a FEG in field emission. We thus pro-

pose a material normal energy distribution (MNED) which embodies the electron density or normal current density as a function of the energy directed towards the surface E_n.

The MNED for the FEG at zero temperature is found by integrating over slices of the Fermi sphere,

$$\frac{dj}{dT_n} = \frac{E_f - T_n}{2\pi^2} = -\frac{1}{2\pi^2}E_n \qquad (1)$$

where $T_n \in [0, E_f]$ is the normal-directed kinetic energy, E_f is the Fermi energy of the material, and E_n is the normal energy relative to the Fermi level. Eqs. (1) and (2) are in Hartree atomic units (a.u.) with $\hbar = m_e = -q_e = 1$.

The MTE (mean transverse energy) as a function of the normal energy is found to be,

$$\text{MTE}(T_n) = \frac{1}{2}(E_f - T_n) = -\frac{1}{2}E_n \qquad (2)$$

and it is conserved in our model between bulk and vacuum due to transverse momentum conservation.

METHODS

We use density-functional theory (DFT) to determine the MNED of real materials through two approaches: slab and bulk calculations. The former is used as a direct, but coarse, calculation of the MNED so that we may verify our bulk calculation results, which attain a much higher resolution by employing some basic assumptions for an indirect approach. This verification is done only for Au (100) and (111).

We use the code JDFTx [6] for all DFT calculations. We use SG15 norm-conserving pseudopotentials [7] for all ions and the Perdew-Burke-Ernzerhof GGA exchange-correlation (XC) functional [8].

Slab System Analysis

The Au (100) and (111) slab systems consist of 15 layers where the outermost 6 layers' positions are optimized. The vacuum separation between the periodic slabs' outermost layers is 46.26 a.u. in length, about 6 lattice constants, before optimization. This slab system allows us to directly calculate the wavefunction decay rate in vacuum, κ, which may then be related to the normal energy (relative to the Fermi level) by $E_n = -\frac{1}{2}\kappa^2 + W$ for bound electronic states. To find a single value for κ for each eigenstate we average the modulus of the wavefunction in the transverse dimensions. We fit an exponential to the wavefunction starting where the potential is within 0.8 eV of vacuum level and ending before the wavefunction's magnitude falls below the noise floor.

Bulk System Analysis

The bulk calculations use a single unit cell with one atom. This is significantly cheaper computationally than the slab system and allows us to use a single DFT calculation for any surface orientation. We find that allowing the lattice to relax results in a roughly unchanged lattice constant and that the band structures produced match previous calculations [9, 10], indicating a good pseudopotential and XC functional choice for gold, copper, and tungsten.

For a given state with crystal momentum $\mathbf{k}$ we stipulate that the total energy E (relative to the Fermi level) and the transverse crystal momentum $\mathbf{k}_\parallel$ are conserved between bulk and vacuum, and we can therefore determine the decay rate of the wavefunction in vacuum simply with $\kappa = \sqrt{2(W - E) + k_\parallel^2}$. This then leads to the normal energy within the material $E_n = T_n - E_f = E - \frac{1}{2}k_\parallel^2$.

The transverse momentum conservation is true up to a reciprocal lattice vector – the inclusion of larger momenta outside the first Brillouin zone (BZ) would, in general, lead to larger transverse kinetic energies and lower normal energies. However, states near the Fermi level, which contribute most to field emission, interact with the lattice weakly and therefore occupy these higher transverse modes less.

The normal current contribution of each state is taken to be $dj = \frac{2}{(2\pi)^3} v_{gn} d^3\mathbf{k}$, with $v_{gn} = \frac{\partial E}{\partial k_\perp}$ the group velocity projected along the surface normal and the factor of 2 accounting for spin degeneracy.

We find the distribution of current with respect to the normal energy by Monte-Carlo integration over the first BZ, using the Wannier interpolation method [11] to find the energy and group velocity. Samples with a negative normal group velocity are discarded as they would not contribute to the tunneling current. When finding the polycrystalline averaged MNED we use a random unit vector as the surface normal for each sample. The MTE is found by taking $\frac{1}{2}k_\parallel^2$ to be the transverse energy of each sample and an average, weighted by the samples' normal current contributions, is done within each normal energy bin. We use about 50 million samples within the first BZ.

RESULTS

The Au MNED density is shown in Fig. 1. The surface and bulk calculations roughly agree with each other in shape, particularly considering that the uncertainty in normal energy for the surface calculations is 0.8 eV due to the potential's non-instantaneous transition to vacuum and our fitting scheme. The Au MNED current matches the FEG result surprisingly well (much like Cu in Fig. 2) while the MNED density does not. By this observation the normal group velocity, or the factor between current and density, cannot follow a simple FEG calculation. We thus have no method of calculating the MNED current for a slab system.

The Cu MNED current and MTE are shown in Fig. 2. The Cu (100), (110), and averaged surfaces agree well with the FEG predictions near the Fermi level. The Cu and Au (111)
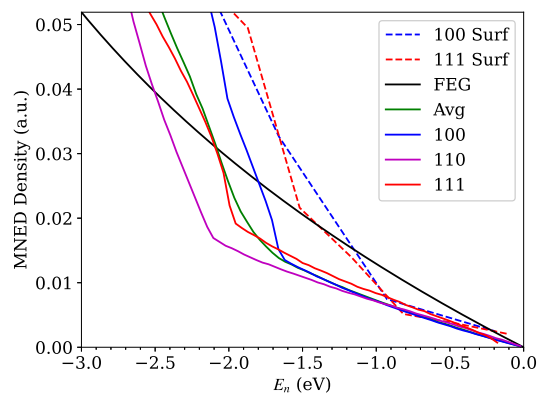

Figure 1: Au MNED source density near the Fermi level at $E_n = 0$. Surface calculations (dashed) for the (100) (blue) and (111) (red) surfaces agree well with their bulk calculation (solid) counterparts, considering their 0.8 eV uncertainty in E_n. The polycrystalline average (green) and (110) surface (magenta) for from the bulk calculations are also included. All cases exhibit FEG-like qualities close to the Fermi level, albeit with a lower density.

MNED currents strongly deviate from the FEG predictions close to the Fermi level. The maximum normal energy attained is less than the Fermi level and the minimum MTE is found to be non-zero due to the Bragg plane intersection of the Fermi surface for these materials in this direction, as we will discuss in the Discussion section.
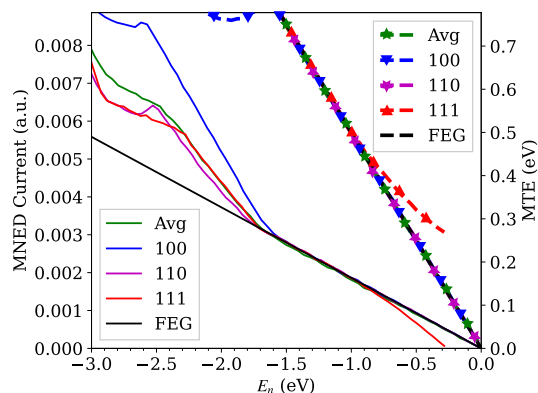

Figure 2: Cu MNED source current (solid) and MTE (dashed) near the Fermi level at $E_n = 0$. The polycrystalline (green), (100) (blue), and (110) (magenta) curves agree surprisingly well with the FEG (black) near the Fermi level. The (111) (red) result notably terminates 0.27 eV below the Fermi level and attains a minimum MTE of 270 meV due to the Fermi surface Bragg plane intersection in this direction.

The W MNED current and MTE are shown in Fig. 3. Tungsten behaves less like a FEG than gold and copper [12] and so we expect these results to deviate further, which is observed. Regardless, the distributions are roughly linear near the Fermi level and may be approximated by a modified

FEG with larger currents, i.e. by multiplying Eqs. (1) and (2) by a constant.

We find these modified FEG constants for the Au, Cu, and W results by fitting a line between the modified Fermi level (at the highest occupied normal energy) and where the linear trend seems to stop at lower normal energies. This data, as well as the increase in work function (due to the modified normal energy Fermi level) and minimum MTE for Au and Cu (111), are summarized in Table 1 for the cases where a deviation from the FEG was observed.
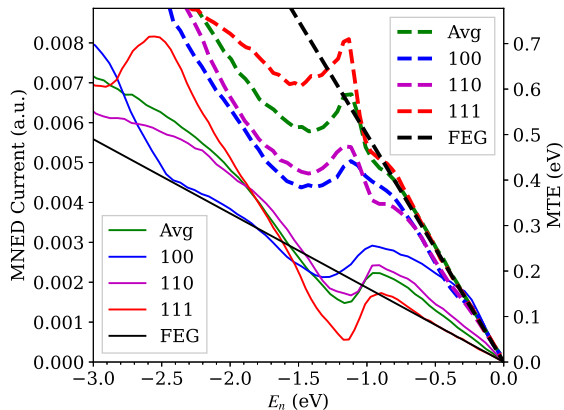

Figure 3: W MNED source current (solid) and MTE (dashed) near the Fermi level at $E_n = 0$. The polycrystalline (green), (100) (blue), and (110) (magenta) curves behave similarly to the FEG (black). The (111) (red) result agrees most with the FEG.

Table 1: Observed MNED current and MTE slopes relative to the slopes for the FEG in Eqs. (1) and (2) respectively, with effective work function increase and minimum MTE contribution for each studied material surface. The fitting is done between the (modified) Fermi level and where the linear trend roughly ceases. "(Avg)" refers to the directionally averaged calculation for polycrystalline materials. For surfaces Au(100), Au(110), Au(Avg), Cu(100), Cu(110), and W(111) no significant deviation from the FEG was found. The W(100) and W(110) surfaces are only fit out to $E_n = -0.13$ eV.

Surface	MNED Slope	MTE Slope	ΔW (eV)	Minimum MTE (meV)
Au(111)	1.25	0.73	0.16	170
Cu(Avg)	0.98	1	-	-
Cu(111)	1.48	0.54	0.27	270
W (Avg)	1.42	1	-	-
W (100)	3.58	1.06	-	-
W (110)	1.92	0.97	-	-

DISCUSSION

The field emission work function anisotropy for Au and Cu (111) surfaces is perhaps the most notable result here. The Fermi surfaces of these metals intersect the (111) Bragg planes [12], which may be understood through the weak binding model. This intersection forms a disc where the total energy is less than the Fermi level everywhere except for the edge where the transverse momentum is non-zero. This indicates that the normal energy is also less than the Fermi level. This feature combined with our model results in an increased effective work function and MTE at and around the (111) surface normal.

Work function anisotropy is a well-studied phenomenon with various methods of measurement, oftentimes with different approaches resulting in different values [13]. It is understood to originate primarily due to the surface disturbance, and not any particular bulk-originating anisotropy [14]. Here we have found a possible bulk-originating work function increase on the order of 100's meV specifically for field emission. This effect compounds with the photoemission work function for the given surface and is comparable to the surface-originating anisotropies.

We otherwise find that, for orientations where there is no Bragg plane intersection, these materials behave akin to a FEG, albeit with more or less total current or MTE near the Fermi level. Of particular note is the large source current for the W(100) surface where we expect about 3.6 times the current we would otherwise get from a pure FEG calculation at low fields. This is quite substantial as, for instance, the choice of potential shape for a Fowler-Nordheim model results in a prefactor which may vary in magnitude by factors on the order of 2 [15], making this observed increase in current impactful for such studies.

CONCLUSION

We found that gold, copper, and tungsten generally abide well by the FEG model for applications in electron field emission. Some orientations of tungsten have a higher electron supply than calculated by a purely FEG calculation, namely the W(100) surface which has nearly 3.6 times the surface current. An orientation-averaged calculation in the spirit of polycrystalline studies also shows good FEG-like behavior as expected. We also find that, for Au and Cu (111) surfaces, the work function and intrinsic MTE are elevated due to the Fermi surfaces' Bragg plane intersections. These results will have a significant impact on the currents calculated using a Fowler-Nordheim model, illuminating the importance of studying even a metallic cathode's electronic distribution.

Future work includes surface calculations of tungsten as well as improved vacuum fitting methods and an increase in sample number by Wannier interpolation. Additionally, the bulk method may be bolstered by some analytical work which may reveal a simpler method of calculating the MNED and MTE slope near the Fermi level. Other common field-emitting materials including semi-conductors are also under consideration.

REFERENCES

[1] A. V. Crewe, M. Isaacson, and D. Johnson, "A simple scanning electron microscope," *Review of Scientific Instruments*, vol. 40, no. 2, pp. 241–246, 1969.

[2] R. Xiang *et al.*, "Experimental studies of dark current in a superconducting rf photoinjector," *Phys. Rev. ST Accel. Beams*, vol. 17, p. 043 401, 2014.

[3] A. C. Keser, T. M. Antonsen, G. S. Nusinovich, D. G. Kashyn, and K. L. Jensen, "Heating of microprotrusions in accelerating structures," *Phys. Rev. ST Accel. Beams*, vol. 16, p. 092 001, 2013.

[4] J. I. Mann, T. Arias, G. E. Lawler, J. K. Nangoi, and J. B. Rosenzweig, "Simulations of Nanoblade-Enhanced Laser-Induced Cathode Emissions and Analyses of Yield, MTE, and Brightness," in *Proc. IPAC'21*, Campinas, Brazil, May 2021, pp. 2957–2960.

[5] R. H. Fowler and L. Nordheim, "Electron emission in intense electric fields," *Proceedings of the Royal Society of London. Series A, Containing Papers of a Mathematical and Physical Character*, vol. 119, no. 781, pp. 173–181, 1928.

[6] "Jdftx: Software for joint density-functional theory," *SoftwareX*, vol. 6, pp. 278–284, 2017.

[7] D. R. Hamann, "Optimized norm-conserving vanderbilt pseudopotentials," *Phys. Rev. B*, vol. 88, p. 085 117, 2013.

[8] J. P. Perdew, K. Burke, and M. Ernzerhof, "Generalized gradient approximation made simple," *Phys. Rev. Lett.*, vol. 77, pp. 3865–3868, 1996.

[9] G. Prandini, A. Marrazzo, I. Castelli, N. Mounet, and N. Marzari, "Precision and efficiency in solid-state pseudopotential calculations," *NPJ Computational Materials*, vol. 4, 2018.

[10] K. Lejaeghere *et al.*, "Reproducibility in density functional theory calculations of solids," *Science*, vol. 351, no. 6280, p. 3000, 2016.

[11] N. Marzari, A. A. Mostofi, J. R. Yates, I. Souza, and D. Vanderbilt, "Maximally localized wannier functions: Theory and applications," *Rev. Mod. Phys.*, vol. 84, pp. 1419–1475, 2012.

[12] Y. P. Gaĭdukov, "Topology of fermi surfaces of metals (reference table)," *Soviet Physics Uspekhi*, vol. 13, no. 2, pp. 194–203, 1970.

[13] H. Kawano, "Effective work functions of the elements: Database, most probable value, previously recommended value, polycrystalline thermionic contrast, change at critical temperature, anisotropic dependence sequence, particle size dependence," *Progress in Surface Science*, vol. 97, no. 1, p. 100 583, 2022.

[14] R. Smoluchowski, "Anisotropy of the electronic work function of metals," *Phys. Rev.*, vol. 60, pp. 661–674, 1941.

[15] R. G. Forbes, "On the need for a tunneling pre-factor in fowler–nordheim tunneling theory," *Journal of Applied Physics*, vol. 103, no. 11, p. 114 911, 2008.

MC3: Novel Particle Sources and Acceleration Techniques

T02: Electron Sources